Composite Structures 93 (2011) 2322–2329

Contents lists available at ScienceDirect

Composite Structures

journal homepage: www.elsevier.com/locate/compstruct

An improved model for naturally curved and twisted composite beams with closed thin-walled sections

A.M. Yu, J.W. Yang, G.H. Nie *, X.G. Yang

School of Aerospace Engineering and Applied Mechanics, Tongji University, Shanghai 200092, PR China

ARTICLE INFO

Article history:
Available online 13 April 2011

Keywords:
Naturally curved and twisted beam
Anisotropic
Eigenwarping
Generalized warping coordinate
Elastic coupling

ABSTRACT

This paper presents an improved model for naturally curved and twisted anisotropic beams with closed thin-walled cross-sections. By introducing eigenwarping functions and expanding axial displacements in series of eigenwarpings, the differential equation involving the generalized warping coordinate and the expression for eigenvalues can be derived using the principle of minimum potential energy. In the model the effects of some factors such as the initial curvature, torsion of the beams as well as torsion-related warping, transverse shear deformations and elastic coupling are incorporated. As an application, the present model is adopted to do an analysis for closed thin-walled composite box beams. Comparison with the existing experimental observation and numerical results shows that the proposed model is valid for analyzing such naturally curved and twisted beams.

1. Introduction

Static and dynamic analysis of naturally curved and twisted beams with closed thin-walled sections made of anisotropic materials has many important applications in mechanical, civil and aeronautical engineering due to their outstanding engineering properties, such as streamlined modeling and favorable loaded characteristics. Helicopter blades and flexible space structures are specific cases of the beams. Some beam theories have been developed for analysis of mechanical behaviors, such as generalized beam theory [1] and refined beam theory [2–5]. The structural behavior of the beams is no longer appropriately modeled with the beam theory for isotropic materials [6–8], and a more advanced theory must be developed. While much has been done in the theories of plates, shells, straight beams and curved beams made of laminated composite materials [9–25], much less has been done in the theory of naturally curved and twisted closed thin-walled beams made of anisotropic materials. There have been some related studies to the application of the finite element method for the beam problem [26–28]. A comprehensive treatment to the warping has been proposed for modeling box beams by using the variational principles, which leads to solution for warping of cross-sections in a corresponding eigenvaule problem [29]. This theory is only valid for the straight beams. For the curved beams, an improved model is needed for incorporating the effects of the initial curvature and torsion of the beams. Recently, using solutions for several characteristic beam elasticity problems from the exact beam theory, characteristic operators in formulation of the model have been treated, which can be used to evaluate effectively the structural behaviors including the warping effect [30].

This paper aims to propose an improved model for naturally curved and twisted composite beams with closed thin-walled sections. By introducing eigenwarping functions and expanding axial displacements in series of eigenwarpings, the differential equation involving the generalized warping coordinate and the expression for eigenvalues can be derived using the principle of minimum potential energy. In the model the effects of some factors such as the initial curvature, torsion of the beams as well as torsion-related warping, transverse shear deformations and elastic coupling are incorporated. Numerical examples are given, and comparison with the existing experimental observation and numerical results shows that the proposed model has enough exactness in computation, and is valid for analysis of naturally curved and twisted anisotropic beams with closed thin-walled cross-sections.

2. Geometry and constitutive relations of the beam

Let the locus of the cross-sectional centroid of the beam be a continuous curve in space denoted by l, and the tangential, normal and bi-normal unit vectors of the curve are denoted by $\boldsymbol{t}$, $\boldsymbol{n}$ and $\boldsymbol{b}$, respectively. The Frenet–Serret formula for a smooth curve is

$$\boldsymbol{t}' = k_1\boldsymbol{n}, \quad \boldsymbol{n}' = -k_1\boldsymbol{t} + k_2\boldsymbol{b}, \quad \boldsymbol{b}' = -k_2\boldsymbol{n}, \tag{1}$$

where superscript prime represents the derivative with respect to s. The symbols s, k_1 and k_2 are arc coordinate, curvature and torsion of the curve, respectively.

* Corresponding author.
E-mail address: ghnie@tongji.edu.cn (G.H. Nie).

0263-8223/$ - see front matter © 2011 Elsevier Ltd. All rights reserved.
doi:10.1016/j.compstruct.2011.03.020

Let us introduce ξ- and η-directions in coincidence with the principal axes through the centroid O_1, as shown in Fig. 1. The angle between the ξ-axis and normal $\boldsymbol{n}$ is represented by θ, which is generally a function of s. If the unit vectors of $O_1\xi$ and $O_1\eta$ are represented by $\boldsymbol{i}_\xi$ and $\boldsymbol{i}_\eta$, then

$$\begin{aligned}\boldsymbol{i}_\xi &= \boldsymbol{n}\cos\theta + \boldsymbol{b}\sin\theta,\\ \boldsymbol{i}_\eta &= -\boldsymbol{n}\sin\theta + \boldsymbol{b}\cos\theta.\end{aligned} \tag{2}$$

From Eq. (1) the following expressions are obtained

$$\begin{aligned}\boldsymbol{t}' &= k_\eta\boldsymbol{i}_\xi - k_\xi\boldsymbol{i}_\eta,\\ \boldsymbol{i}'_\xi &= -k_\eta\boldsymbol{t} + k_s\boldsymbol{i}_\eta,\\ \boldsymbol{i}'_\eta &= k_\xi\boldsymbol{t} - k_s\boldsymbol{i}_\xi,\end{aligned} \tag{3}$$

in which $k_\xi = k_1\sin\theta$, $k_\eta = k_1\cos\theta$, $k_s = k_2 + \theta$.

A geometry of cross-section of the beam is shown in Fig. 2. The ζ is the curvilinear coordinate describing the contour of the section, denoted by C. It is assumed that the contour remains unchanged, i.e., the cross-section does not deform in its own plane, but the plane allows a warping deformation along its axis. The deformation of the beam is thus governed by six rigid body modes, namely, three translations of the section, $u_s(s)$, $u_\xi(s)$, $u_\eta(s)$, and three rotations of the section, $\varphi_s(s)$, $\varphi_\xi(s)$ and $\varphi_\eta(s)$. The membrane stresses in the beam are composed of an axial stress flow n and a shear stress flow q. These two stress flows are acting in the plane of contour and are uniform across the thickness of the beam. The constitutive relations for a thin-walled laminated beam are expressed by [29].

$$\begin{bmatrix} n \\ q \end{bmatrix} = \begin{bmatrix} A_{nn} & A_{nq} \\ A_{nq} & A_{qq} \end{bmatrix}\begin{bmatrix} e \\ \gamma \end{bmatrix}, \tag{4}$$

in which the e and γ are the membrane axial strain and (engineering) shear strain, respectively, and $A_{nn} = A_{11} - A_{12}^2/A_{22}; A_{qq} = A_{66} - A_{26}^2/A_{22}; A_{nq} = A_{16} - A_{12}A_{26}/A_{22}$, and $A_{ij} = \sum_{k=1}^{n}\int_{z_{k-1}}^{z_k}\overline{Q}_{ij}dz$ $(i = 1, 2, 6)$ where $\overline{Q}_{ij}$ are expressed by [31]

$$\begin{bmatrix} \overline{Q}_{11} \\ \overline{Q}_{22} \\ \overline{Q}_{12} \\ \overline{Q}_{66} \\ \overline{Q}_{16} \\ \overline{Q}_{26} \end{bmatrix} = \begin{bmatrix} l^4 & m^4 & 2l^2m^2 & 4l^2m^2 \\ m^4 & l^4 & 2l^2m^2 & 4l^2m^2 \\ l^2m^2 & l^2m^2 & l^4+m^4 & -4l^2m^2 \\ l^2m^2 & l^2m^2 & -2l^2m^2 & (l^2-m^2)^2 \\ l^3m & -lm^3 & lm^3-l^3m & 2(lm^3-l^3m) \\ lm^3 & -l^3m & l^3m-lm^3 & 2(l^3m-lm^3) \end{bmatrix}\begin{bmatrix} Q_{11} \\ Q_{22} \\ Q_{12} \\ Q_{66} \end{bmatrix}$$

where l, m are direct cosine and

$$\begin{aligned}&Q_{11} = (1-\upsilon_{LT}\upsilon_{TL})^{-1}E_L, Q_{22} = (1-\upsilon_{LT}\upsilon_{TL})^{-1}E_T, Q_{66} = G_{LT},\\ &Q_{12} = Q_{21} = (1-\upsilon_{LT}\upsilon_{TL})^{-1}\upsilon_{LT}E_L.\end{aligned}$$

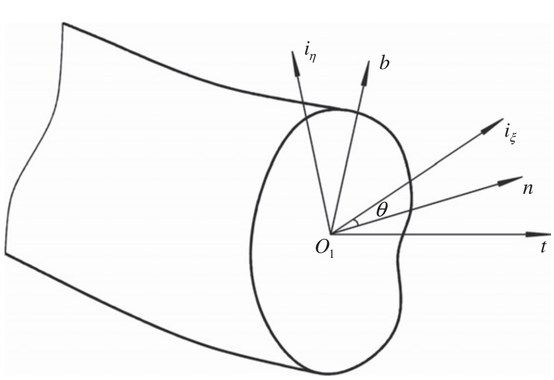

Fig. 1. Geometry of the cross-section.

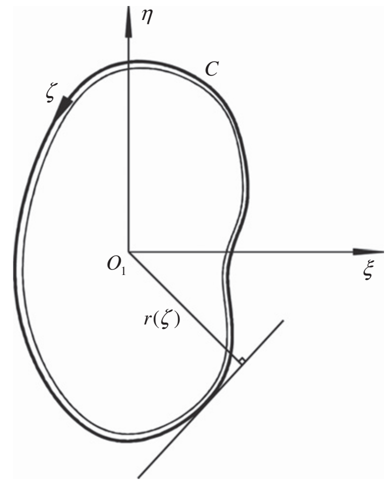

Fig. 2. Closed cell thin-walled beam model.

3. Equilibrium equations

Simplifying stress vectors to the centroid O_1 on the cross-section A, as shown in Fig. 3, the principal vector $\boldsymbol{Q}(Q_s, Q_\xi, Q_\eta)$ and principal moment $\boldsymbol{M}(M_s, M_\xi, M_\eta)$ are written by

$$\boldsymbol{Q} = Q_s\boldsymbol{t} + Q_\xi\boldsymbol{i}_\xi + Q_\eta\boldsymbol{i}_\eta, \quad \boldsymbol{M} = M_s\boldsymbol{t} + M_\xi\boldsymbol{i}_\xi + M_\eta\boldsymbol{i}_\eta,$$

where Q_s is axial force, Q_ξ and Q_η are two shear forces while M_s is torque, M_ξ and M_η are bending moments. The external forces and moments per unit length along the beam axis are indicated by $\boldsymbol{p}$ and $\boldsymbol{m}$ as

$$\boldsymbol{p} = p_s\boldsymbol{t} + p_\xi\boldsymbol{i}_\xi + p_\eta\boldsymbol{i}_\eta, \boldsymbol{m} = m_s\boldsymbol{t} + m_\xi\boldsymbol{i}_\xi + m_\eta\boldsymbol{i}_\eta.$$

The equilibrium equations are

$$\begin{aligned}&\frac{d}{ds}\{Q\} - [K]\cdot\{Q\} + \{p\} = \{0\},\\ &\frac{d}{ds}\{M\} - [K]\cdot\{M\} - [H]\cdot\{Q\} + \{m\} = \{0\},\end{aligned} \tag{5}$$

where

$$\{Q\} = \begin{bmatrix} Q_s & Q_\xi & Q_\eta \end{bmatrix}^T, \quad \{M\} = \begin{bmatrix} M_s & M_\xi & M_\eta \end{bmatrix}^T,$$

$$\{p\} = \begin{bmatrix} p_s & p_\xi & p_\eta \end{bmatrix}^T, \quad \{m\} = \begin{bmatrix} m_s & m_\xi & m_\eta \end{bmatrix}^T,$$

$$[K] = \begin{bmatrix} 0 & k_\eta & -k_\xi \\ -k_\eta & 0 & k_s \\ k_\xi & -k_s & 0 \end{bmatrix}, \quad [H] = \begin{bmatrix} 0 & 0 & 0 \\ 0 & 0 & 1 \\ 0 & -1 & 0 \end{bmatrix}.$$

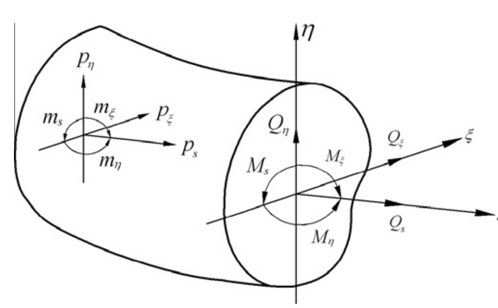

Fig. 3. Stress resultants in a typical beam element.

The general solutions have the following forms [32]:

$$\{Q\} = [A]\cdot\left(\{Q_0\} - \int_0^s [A]^T\cdot\{p\}ds\right),$$
$$\{M\} = [A]\cdot\left\{\{M_0\} + \int_0^s [A]^T\cdot([H]\cdot[A]\cdot(\{Q_0\}+\{Q^*\}) - \{m\})ds\right\}, \tag{6}$$

where $\{Q_0\}$ and $\{M_0\}$ are column matrices for integration constants, and $\{Q^*\} = -\int_0^s [A]^T\cdot\{p\}ds$ in which $[A]$ is the matrix of direction cosine with each element being dot product of two corresponding unit vectors for both coordinate system characterized by $\boldsymbol{t}$, $\boldsymbol{i}_\xi$, $\boldsymbol{i}_\eta$ and $\boldsymbol{i}_x$, $\boldsymbol{i}_y$, $\boldsymbol{i}_z$ respectively expressed by

$$[A] = \begin{bmatrix} t\cdot i_x & t\cdot i_y & t\cdot i_z \\ i_\xi\cdot i_x & i_\xi\cdot i_y & i_\xi\cdot i_z \\ i_\eta\cdot i_x & i_\eta\cdot i_y & i_\eta\cdot i_z \end{bmatrix}. \tag{7}$$

4. Mathematical formulation for the eigenwarping approach

In eigenwarping approach, the solution for the problem will be determined by adding eigenwarping in the form of a series expansion to a warping-free solution. The warping of cross-sections is determined by a solution for a corresponding eigenvaule problem. The eigenvaule problem can be tackled using a discretized element method based on the discretization for eigenwarping function over the section of the beams [29].

Assuming that the deformation of the beam consists of stretching, bending and torsion, thus the displacement field neglecting the effect of warping can be written as follows

$$\boldsymbol{u} = W\boldsymbol{t} + U\boldsymbol{i}_\xi + V\boldsymbol{i}_\eta, \tag{8}$$

in which

$$\begin{aligned} W &= u_s(s) + \eta\varphi_\xi(s) - \xi\varphi_\eta(s),\\ U &= u_\xi(s) - \eta\varphi_s(s),\\ V &= u_\eta(s) + \xi\varphi_s(s). \end{aligned} \tag{9}$$

The strain–displacement relations are [6]

$$\begin{aligned} \sqrt{g}e_{11or} &= \varepsilon_s + \eta\omega_\xi - \xi\omega_\eta,\\ 2\sqrt{g}e_{12or} &= \varepsilon_\xi - \eta\omega_s,\\ 2\sqrt{g}e_{13or} &= \varepsilon_\eta + \xi\omega_s, \end{aligned} \tag{10}$$

In these equations,

$$\begin{aligned} &\varepsilon_s = u_s' - k_\eta u_\xi + k_\xi u_\eta, \quad \varepsilon_\xi = u_\xi' + k_\eta u_s - k_s u_\eta - \varphi_\eta,\\ &\varepsilon_\eta = u_\eta' - k_\xi u_s + k_s u_\xi + \varphi_\xi, \quad \omega_s = \varphi_s' - k_\eta\varphi_\xi + k_\xi\varphi_\eta,\\ &\omega_\xi = \varphi_\xi' + k_\eta\varphi_s - k_s\varphi_\eta, \quad \omega_\eta = \varphi_\eta' - k_\xi\varphi_s + k_s\varphi_\xi. \end{aligned} \tag{11}$$

The above equation is usually referred to as geometry equations, and can be rewritten as

$$\begin{aligned} &\frac{d}{ds}\{\varphi\} - [K]\{\varphi\} - \{\omega\} = \{0\},\\ &\frac{d}{ds}\{u\} - [K]\cdot\{u\} - [H]\cdot\{\varphi\} - \{\varepsilon\} = \{0\}, \end{aligned} \tag{12}$$

where

$$\{\varphi\} = [\varphi_s\ \varphi_\xi\ \varphi_\eta]^T, \{u\} = [u_s\ u_\xi\ u_\eta]^T,$$
$$\{\omega\} = [\omega_s\ \omega_\xi\ \omega_\eta]^T, \{\varepsilon\} = [\varepsilon_s\ \varepsilon_\xi\ \varepsilon_\eta]^T,$$

so the general solutions to the geometry equations are [32]

$$\{\varphi\} = [A]\cdot(\{\varphi_0\} + \{\varphi^*\}),$$
$$\{u\} = [A]\cdot\left\{\{U_0\} + \int_0^s [A]^T\cdot(\{\varepsilon\} + [H]\cdot[A](\{\varphi_0\}+\{\varphi^*\}))ds\right\}, \tag{13}$$

in which $\{\varphi_0\}$ and $\{U_0\}$ are integration constants, $\{\varphi^*\} = \int_0^s [A]^T\cdot\{\omega\}ds$. For simplicity, the initial curvature k_1 is assumed to be small, because $k_\xi = k_1\sin\theta$, $k_\eta = k_1\cos\theta$, then $g = (1 - \xi k_\eta + \eta k_\xi)^2$ gives

$\sqrt{g} \approx 1$.

The above equation is realistic for most practical applications. The strains e, γ in Eq. (4) can be written using Eq. (10) as

$$\begin{aligned} e &= e_{11or} = \varepsilon_s + \eta\omega_\xi - \xi\omega_\eta,\\ \gamma &= 2e_{12or}\frac{d\xi}{d\zeta} + 2e_{13or}\frac{d\eta}{d\zeta} = \varepsilon_\xi\frac{d\xi}{d\zeta} + \varepsilon_\eta\frac{d\eta}{d\zeta} + r\omega_s. \end{aligned} \tag{14}$$

According to the relation between the internal forces and stress flows defined by

$$\begin{aligned} &Q_s = \int_C n_{or}d\zeta, \quad M_s = \int_C q_{or}rd\zeta,\\ &Q_\xi = \int_C q_{or}\frac{d\xi}{d\zeta}d\zeta, \quad M_\xi = \int_C n_{or}\eta d\zeta,\\ &Q_\eta = \int_C q_{or}\frac{d\eta}{d\zeta}d\zeta, \quad M_\eta = -\int_C n_{or}\xi d\zeta, \end{aligned} \tag{15}$$

using Eqs. (4) and (14), Eq. (15) changes to

$$\begin{aligned} &Q_s = S\varepsilon_s,\\ &Q_\xi = G_\xi A_{\xi\xi}\varepsilon_\xi + G_\eta A_{\xi\eta}\varepsilon_\eta + \textstyle\int_C A_{qq}r\frac{d\xi}{d\zeta}d\zeta\omega_s,\\ &Q_\eta = G_\xi A_{\xi\eta}\varepsilon_\xi + G_\eta A_{\eta\eta}\varepsilon_\eta + \textstyle\int_C A_{qq}r\frac{d\eta}{d\zeta}d\zeta\omega_s,\\ &M_s = I_P\omega_s + \textstyle\int_C A_{qq}r\frac{d\xi}{d\zeta}d\zeta\varepsilon_\xi + \int_C A_{qq}r\frac{d\eta}{d\zeta}d\zeta\varepsilon_\eta,\\ &M_\xi = I_{\xi\xi}\omega_\xi,\\ &M_\eta = I_{\eta\eta}\omega_\eta, \end{aligned} \tag{16}$$

where G_ξ and G_η are the shear coefficients in ξ- and η-directions for closed thin-walled composite beams [33]; $S = \int_C A_{nn}d\zeta$ is the axial stiffness, and $I_{\xi\xi} = \int_C A_{nn}\eta^2 d\zeta$ is the bending stiffness (similar definition for $I_{\eta\eta}$), $A_{\xi\xi} = \int_C A_{qq}\left(\frac{d\xi}{d\zeta}\right)^2 d\zeta$ is the shear stiffness (similar definitions for $A_{\eta\eta}$ and $A_{\xi\eta}$), and $I_P = \int_C A_{nn}r^2 d\zeta$ is the torsional stiffness. In above derivation, the equations $\int_C A_{nn}\xi d\zeta = \int_C A_{nn}\eta d\zeta = \int_C A_{nn}\xi\eta d\zeta = 0$, have been applied. The six strain measures ε_s, ε_ξ, ε_η, ω_s, ω_ξ, ω_η in Eq. (16) can be evaluated by the internal forces determined from Eq. (6). Using the resulting strain measures, the strains e and γ and stress flows n and q can be obtained from Eqs. (14) and (4), respectively. The displacements in Eq. (8) can be also determined using Eq. (13).

In the following let us consider the effect of warping. For an unloaded beam, i.e., $\boldsymbol{p} = \boldsymbol{m}$=0, an additional part of solution for the displacement in the axial direction and three strain measures is assumed to be in the form of

$$\begin{aligned} W_{co}(\zeta, s) &= \varphi(\zeta)\alpha(s),\\ \varepsilon_{\xi co}(s) &= \overline{U}\alpha(s),\\ \varepsilon_{\eta co}(s) &= \overline{V}\alpha(s),\\ \omega_{sco}(s) &= \overline{\Xi}\alpha(s), \end{aligned} \tag{17}$$

where $\varphi(\zeta)$ and $\alpha(s)$ are the eigenwarping modes of the cross-section and the generalized warping coordinates, respectively, and $\overline{U}, \overline{V}$ and $\overline{\Xi}$ are three unknown parameters. Substituting Eq. (17) into the strain–displacement relations incorporating the warping effect [6,34], yields

$$\begin{aligned} e_{11co} &= \varphi(\zeta)\alpha'(s) + k_s\left[\left(\frac{\partial\varphi}{\partial\xi}\right)\eta - \left(\frac{\partial\varphi}{\partial\eta}\right)\xi\right]\alpha(s),\\ \gamma_{co} &= 2e_{12co}\frac{d\xi}{d\zeta} + 2e_{13co}\frac{d\eta}{d\zeta}\\ &= \overline{U}\alpha(s)\frac{d\xi}{d\zeta} - \eta\overline{\Xi}\alpha(s)\frac{d\xi}{d\zeta} + \left[\left(\frac{\partial\varphi}{\partial\xi}\right) + k_\eta\varphi\right]\alpha(s)\frac{d\xi}{d\zeta}\\ &\quad + \overline{V}\alpha(s)\frac{d\eta}{d\zeta} + \xi\overline{\Xi}\alpha(s)\frac{d\eta}{d\zeta} + \left[\left(\frac{\partial\varphi}{\partial\eta}\right) - k_\xi\varphi\right]\alpha(s)\frac{d\eta}{d\zeta}\\ &= \left(\frac{d\varphi}{d\zeta} - k_\xi\varphi\frac{d\eta}{d\zeta} + k_\eta\varphi\frac{d\xi}{d\zeta} + \overline{U}\frac{d\xi}{d\zeta} + \overline{V}\frac{d\eta}{d\zeta} + r\overline{\Xi}\right)\alpha(s), \end{aligned} \tag{18}$$

where r is the distance from the centroid O_1 to the tangent to the cross-sectional curve, as shown in Fig. 2. For orthotropic beam whose two axes of orthotropy are parallel to the axis of the beam and the tangent, $A_{16} = A_{26} = 0$, resulting in $A_{nq} = 0$, which indicates vanishing of the in-plane extension-shearing coupling of the laminate. The corresponding strain energy is

$$\Pi_{co} = \frac{1}{2}\int_0^l \int_C (A_{nn}e_{11co}^2 + A_{qq}\gamma_{co}^2)d\zeta ds,$$

The expression for eigenvalues can be derived by minimizing the energy with respect to $\varphi, \overline{U}, \overline{V}$ and $\overline{\Xi}$. The associated eigenvalues μ_i^2 can be obtained in the form of a Rayleigh quotient below

$$\mu_i^2 = \frac{\int_C A_{qq}\left\{\left(\frac{d\varphi_i}{d\zeta} - k_\xi\varphi_i\frac{d\eta}{d\zeta} + k_\eta\varphi_i\frac{d\xi}{d\zeta} + \overline{U}_i\frac{d\xi}{d\zeta} + \overline{V}_i\frac{d\eta}{d\zeta} + \overline{\Xi}_i r\right)^2 + \frac{A_{nn}}{A_{qq}}k_s^2\left[\left(\frac{\partial\varphi_i}{\partial\xi}\right)\eta - \left(\frac{\partial\varphi_i}{\partial\eta}\right)\xi\right]^2\right\}d\zeta}{\int_C A_{nn}\varphi_i^2 d\zeta}, \tag{19}$$

where $\overline{U}_i, \overline{V}_i, \overline{\Xi}_i$ are determined by

$$\begin{aligned} &\int_C A_{qq}\sum\left(W_i\frac{d\varphi_i}{d\zeta} - k_\xi W_i\varphi_i\frac{d\eta}{d\zeta} + k_\eta W_i\varphi_i\frac{d\xi}{d\zeta} + \overline{U}_i\frac{d\xi}{d\zeta} + \overline{V}_i\frac{d\eta}{d\zeta} + \overline{\Xi}_i r\right)\frac{d\xi}{d\zeta}d\zeta = 0\\ &\int_C A_{qq}\sum\left(W_i\frac{d\varphi_i}{d\zeta} - k_\xi W_i\varphi_i\frac{d\eta}{d\zeta} + k_\eta W_i\varphi_i\frac{d\xi}{d\zeta} + \overline{U}_i\frac{d\xi}{d\zeta} + \overline{V}_i\frac{d\eta}{d\zeta} + \overline{\Xi}_i r\right)\frac{d\eta}{d\zeta}d\zeta = 0\\ &\int_C A_{qq}\sum\left(W_i\frac{d\varphi_i}{d\zeta} - k_\xi W_i\varphi_i\frac{d\eta}{d\zeta} + k_\eta W_i\varphi_i\frac{d\xi}{d\zeta} + \overline{U}_i\frac{d\xi}{d\zeta} + \overline{V}_i\frac{d\eta}{d\zeta} + \overline{\Xi}_i r\right)r d\zeta = 0 \end{aligned} \tag{20}$$

where

$$\varphi_i = \begin{cases} \frac{s-s_{i-1}}{h} & s_{i-1} \leqslant s \leqslant s_i\\ \frac{s_{i+1}-s}{h} & s_i \leqslant s \leqslant s_{i+1}\\ 0 & \text{other} \end{cases} \tag{21}$$

in which s_i corresponds to the discretized point along the contour of the section denoted by C (see also Fig. 2). In above derivation the following set of orthonormality relations

$$\int_C A_{nn}\varphi_i\varphi_j d\zeta = \delta_{ij}, \quad \int_C A_{qq}\Gamma_i\Gamma_j d\zeta = \mu^2\delta_{ij}, \tag{22}$$

where

$$\Gamma = \sqrt{\left(\frac{d\varphi_i}{d\zeta} - k_\xi\varphi_i\frac{d\eta}{d\zeta} + k_\eta\varphi_i\frac{d\xi}{d\zeta} + \overline{U}_i\frac{d\xi}{d\zeta} + \overline{V}_i\frac{d\eta}{d\zeta} + \overline{\Xi}_i r\right)^2 + \frac{A_{nn}}{A_{qq}}k_s^2\left[\left(\frac{\partial\varphi_i}{\partial\xi}\right)\eta - \left(\frac{\partial\varphi_i}{\partial\eta}\right)\xi\right]^2},$$

have been used, and the products of the generalized warping coordinate and their derivative are eliminated due to small displacement theory. The resulting Eq. (19) contains the terms related to the initial curvature and torsion of the beam, which can be applied to analysis of such naturally curved and twisted beams.

5. Improved beam model and equivalent constitutive equations

Using Eqs. (9), (11) and (17) , the combined displacement in the axial direction and three strain measures can be expressed by

$$W_{im} = W + W_{co} = W + \sum_i \varphi_i(\zeta)\alpha_i(s), \tag{23}$$

$$\begin{aligned} \varepsilon_{\xi im} &= \varepsilon_\xi + \varepsilon_{\xi co} = \varepsilon_\xi + \sum_i \overline{U}_i\alpha_i(s),\\ \varepsilon_{\eta im} &= \varepsilon_\eta + \varepsilon_{\eta co} = \varepsilon_\eta + \sum_i \overline{V}_i\alpha_i(s),\\ \omega_{sim} &= \omega_s + \omega_{sco} = \omega_s + \sum_i \overline{\Xi}_i\alpha_i(s), \end{aligned} \tag{24}$$

Thus, the total strain components e and γ are

$$\begin{aligned} e &= e_{11or} + \sum_i\left\{\varphi_i(\zeta)\alpha_i'(s) + k_s\left[\left(\frac{\partial\varphi_i}{\partial\xi}\right)\eta - \left(\frac{\partial\varphi_i}{\partial\eta}\right)\xi\right]\alpha_i(s)\right\},\\ \gamma &= 2e_{12or}\frac{d\xi}{d\zeta} + 2e_{13or}\frac{d\eta}{d\zeta} + \sum_i\left(\frac{d\varphi_i}{d\zeta} - k_\xi\varphi_i\frac{d\eta}{d\zeta} + k_\eta\varphi_i\frac{d\xi}{d\zeta}\right.\\ &\quad \left. + \overline{U}_i\frac{d\xi}{d\zeta} + \overline{V}_i\frac{d\eta}{d\zeta} + r\overline{\Xi}_i\right)\alpha_i(s). \end{aligned} \tag{25}$$

The total potential energy for the beam

$$\Pi = \frac{1}{2}\int_0^l \int_C (A_{nn}e^2 + A_{qq}\gamma^2)d\zeta ds - \int_0^l (p_\xi u_\xi + p_\eta u_\eta + m_s\varphi_s)ds, \tag{26}$$

Using the orthonormality relationships (17), Eq. (26) changes to

$$\Pi = \Pi_{or} + \sum_i \int_0^l \left[\frac{1}{2}(\alpha_i'^2 + \mu_i^2\alpha_i^2) - d_i\alpha_i\right]ds, \tag{27}$$

where

$$d_i = Q_\xi(\overline{U}_i + k_\eta\varphi_i) + Q_\eta(\overline{V}_i - k_\xi\varphi_i) + M_s\overline{\Xi}_i. \tag{28}$$

The Π_{or} is the energy for the warping-free beam. The second term in Eq. (27) indicates that $\varphi, \overline{U}, \overline{V}$ and $\overline{\Xi}$ are independent of the previous six rigid body modes corresponding to the warping-free beam. Minimizing Π_{or} will result in the equilibrium Eq. (5), and minimizing the second terms with respect to α_i yields

$$\alpha_i'' - \mu_i^2\alpha_i = -d_i. \tag{29}$$

The above equation is solved easily. Accordingly, the improved solution for the problem in terms of the series expansion of eigenwarping takes the form of

$$
\begin{aligned}
&W_{im} = W + \sum_i \varphi_i \alpha_i, \quad \varepsilon_{\xi im} = \varepsilon_\xi + \sum_i \overline{U}_i \alpha_i,\\
&\varepsilon_{\eta im} = \varepsilon_\eta + \sum_i \overline{V}_i \alpha_i, \quad \omega_{sim} = \omega_s + \sum_i \overline{\Xi}_i \alpha_i,\\
&n_{im} = n + \sum_i A_{nn}\left\{\varphi_i(\zeta)\alpha_i'(s) + k_s\left[\left(\frac{\partial \varphi_i}{\partial \xi}\right)\eta - \left(\frac{\partial \varphi_i}{\partial \eta}\right)\xi\right]\alpha_i(s)\right\},\\
&q_{im} = q + \sum_i A_{qq}\left(\frac{d\varphi_i}{d\zeta} - k_\xi \varphi_i \frac{d\eta}{d\zeta} + k_\eta \varphi_i \frac{d\xi}{d\zeta} + \overline{U}_i \frac{d\xi}{d\zeta} + \overline{V}_i \frac{d\eta}{d\zeta} + r\overline{\Xi}_\imath\right)\alpha_i(s).
\end{aligned}
\tag{30}
$$

6. Example analysis

For the purpose of computation, a curved, thin-walled composite box beam fixed at one end ($s = 0$) and free at the other end ($s = l$), as shown in Fig. 4, is considered as computational model. The axis of the beam is assumed to be a circular arc with radius a. In this case there is

$$
\begin{aligned}
&\beta = \frac{l}{a}, \quad k_\eta = k_1 = \frac{1}{a},\\
&x = a\sin\beta, \quad y = a(1-\cos\beta),
\end{aligned}
$$

and $\theta = k_s = k_\xi = 0$ and $k_\eta = 1/R$. The external load is assumed to be uniformly distributed load p_η in the η-direction, i.e.,

$$
\{p\} = [0\ 0\ p_\eta]^T, \quad \{m\} = [0\ 0\ 0]^T.
$$

Using Eqs. (6) and (13), the expressions related to the internal forces and displacements are

$$
\begin{aligned}
&M_s = M_{0s}\cos\beta + M_{0\xi}\sin\beta + Q_{0\eta}a(1-\cos\beta) + p_\eta a^2(\sin\beta - \beta),\\
&M_\xi = -M_{0s}\sin\beta + M_{0\xi}\cos\beta + Q_{0\eta}a\sin\beta - p_\eta a^2(1-\cos\beta),\\
&Q_\eta = Q_{0\eta} - p_\eta s,\\
&\varphi_s = \varphi_{0s}\cos\beta + \varphi_{0\xi}\sin\beta + a\cos\beta\int_0^\beta(\omega_s\cos\beta - \omega_\xi\sin\beta)d\beta +\\
&\quad + a\sin\beta\int_0^\beta(\omega_s\sin\beta + \omega_\xi\cos\beta)d\beta,\\
&\varphi_\xi = -\varphi_{0s}\sin\beta + \varphi_{0\xi}\cos\beta - a\sin\beta\int_0^\beta(\omega_s\cos\beta - \omega_\xi\sin\beta)d\beta +\\
&\quad + a\cos\beta\int_0^\beta(\omega_s\sin\beta + \omega_\xi\cos\beta)d\beta,\\
&u_\eta = U_{0\eta} + \varphi_{0s}y - \varphi_{0\xi}x + a\int_0^\beta \varepsilon_\eta d\beta +\\
&\quad + a\int_0^\beta\left[a\sin\beta\int_0^\beta(\omega_s\cos\beta - \omega_\xi\sin\beta)d\beta - a\cos\beta\int_0^\beta(\omega_s\sin\beta + \omega_\xi\cos\beta)d\beta\right]d\beta,
\end{aligned}
\tag{31}
$$

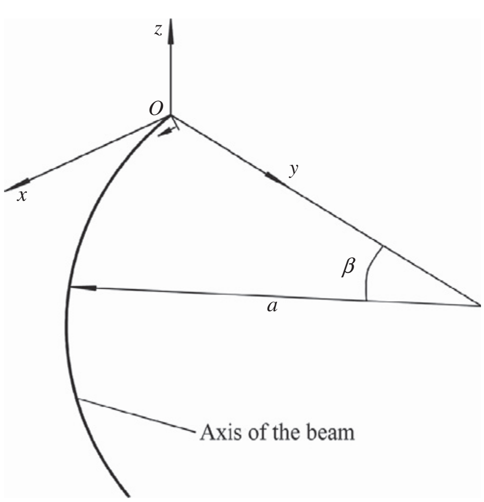

Fig. 4. Geometry of a plane curved beam.

where M_{0s}, $M_{0\xi}$, $Q_{0\eta}$ and φ_{0s}, $\varphi_{0\xi}$, $U_{0\eta}$ are the values of M_s, M_ξ, Q_η and φ_s, φ_ξ, u_η at the end $s = 0$, respectively.

For the uniformly distributed load, p_η, Eq. (29) is rewritten by

$$
\alpha_i'' - \mu_i^2\alpha_i = -p_\eta a\overline{V}_i\left(\frac{\pi}{2} - \beta\right) - p_\eta a^2\overline{\Xi}_i\left(\frac{\pi}{2} - \beta - cos\beta\right). \tag{32}
$$

The form of the solution of Eq. (32) is

$$
\begin{aligned}
\alpha_i = {}& C_1 e^{\mu_i s} + C_2 e^{-\mu_i s} + \frac{1}{\mu_i^2}p_\eta a\overline{V}_i\left(\frac{\pi}{2} - \beta\right) + \frac{1}{\mu_i^2}p_\eta a^2\overline{\Xi}_i\left(\frac{\pi}{2} - \beta\right)\\
&- \frac{1}{\left(\frac{1}{a^2} + \mu_i^2\right)}p_\eta a^2\overline{\Xi}_i cos\beta.
\end{aligned}
\tag{33}
$$

where C_1,C_2 are unknown constants. Using the boundary conditions

$$
\begin{aligned}
&s = 0(\beta = 0), U_{0s} = U_{0\xi} = U_{0\eta} = 0, \varphi_{0s} = \varphi_{0\xi} = \varphi_{0\eta} = 0, \alpha_i = 0,\\
&s = l(\beta = \beta_l), M_s = M_\xi = Q_\eta = 0, \alpha_i' = 0,
\end{aligned}
$$

from Eqs. (31) and (33), yields

$$
\begin{aligned}
&M_{0s} = p_\eta a^2\left(\frac{\pi}{2} - 1\right), \quad M_{0\xi} = -p_\eta a^2, \quad Q_{0\eta} = \frac{\pi}{2}p_\eta a,\\
&C_1 = \left[-\frac{1}{2}\frac{a^3\mu_i^3\pi + \mu_i\pi a - 2e^{\frac{1}{2}\mu_i\pi a}\mu_i^2 a^2 - 2e^{\frac{1}{2}\mu_i\pi a}}{(1 + e^{\mu_i\pi a})\mu_i^3(\mu_i^2 a^2 + 1)}\overline{V}_i\right.\\
&\qquad \left. - \frac{1}{2}\frac{a^4\mu_i^3\pi + a^2\mu_i\pi - 2a^4\mu_i^3 - 2e^{\frac{1}{2}\mu_i\pi a}a}{(1 + e^{\mu_i\pi a})\mu_i^3(\mu_i^2 a^2 + 1)}\overline{\Xi}_i\right]p_\eta,\\
&C_2 = \left[-\frac{1}{2}e^{\frac{1}{2}\mu_i\pi a}\frac{e^{\frac{1}{2}\mu_i\pi a}a^3\mu_i^3\pi + e^{\frac{1}{2}\mu_i\pi a}a\mu_i\pi + 2\mu_i^2 a^2 + 2}{\mu_i^3(1 + e^{\mu_i\pi a})(\mu_i^2 a^2 + 1)}\overline{V}_i\right.\\
&\qquad \left. - \frac{1}{2}e^{\frac{1}{2}\mu_i\pi a}\frac{e^{\frac{1}{2}\mu_i\pi a}a^4\mu_i^3\pi + e^{\frac{1}{2}\mu_i\pi a}a^2\mu_i\pi - 2e^{\frac{1}{2}\mu_i\pi a}a^4\mu_i^3 + 2a}{\mu_i^3(1 + e^{\mu_i\pi a})(\mu_i^2 a^2 + 1)}\overline{\Xi}_i\right]p_\eta.
\end{aligned}
\tag{34}
$$

The above equations will be used in numerical computation.

6.1. Convergence analysis of present model

To evaluate the structural behaviors, a more exact calculation of eigenvalues μ_i^2 in Eq. (19) is of importance to determination on warping coordinate α_i by Eq. (29). Consider a Graphite/Epoxy box beam for the lay-up $(0°/90°)_3$ with length $l = 30.0$ in., and height and width of cross-section of the beam are $h = 0.537$ in. and $c = 0.953$ in., respectively. Some elastic properties are given as $E_L = 20.59$ msi, $E_T = 1.42$ msi, $G_{LT} = 0.87$ msi and $\upsilon_{LT} = 0.42$ [35]. The four edges of the cross-section are discretized to 1484, 2968, 3200 and 3500 elements, respectively. Different discretization will result in corresponding values of eigenvalues for μ_i^2. The first ten eigenvalues of μ_i^2 for different elements are listed in Table 1. The result indicates that when the number of discretized element is large enough, e.g., it is close to 3200, the eigenvalues have enough exactness in computation.

Table 1
First 10 eigenvalues for different discretized elements.

Elements	Eigenvalues (μ_i^2)				
	1	2	3	4	5
1484	1.93E−11	2.57E−12	5.01E−12	1.3226	1.4041
2968	9.38E−12	3.11E−11	5.34E−11	1.3225	1.4040
3200	3.25E−10	1.49E−10	9.75E−11	1.3225	1.4041
3500	1.16E−10	5.78E−11	2.27E−10	1.3225	1.4041
	6	7	8	9	10
1484	2.3764	3.1522	5.559	5.6164	8.3641
2968	2.3763	3.1521	5.5588	5.6162	8.3636
3200	2.3763	3.1521	5.5588	5.6162	8.3637
3500	2.3763	3.1521	5.5588	5.6162	8.3636

6.2. Comparison of results for present model with available data

A comparison of the span-wise distributions of bending slope is listed in Table 2 for uncoupled cross-ply beams subjected to unit tip bending load when the ratio of the length of the beam to the height of the cross section is prescribed to be 29 [35]. It is observed that present result is more close to the analytical solution [35] and experimental data [36,37]. A comparatively lager error is seen when compared with the finite element results [38]. Similar result for twist angle to unit tip torque for the same lay-up is shown from Table 3. In Table 4 the span-wise distribution of bending slope is illustrated for symmetric lay-up beams (i.e., top and bottom $(45°)_6$, sides $(45°/-45°)_3$) subjected to a tip bending load where the ratio of the length of the beam to the height of the cross-section is prescribed to be 56 [35]. The result indicates that the present model shows good accuracy in computation compared with available results.

For a beam with curvature $k = 0.5$ and 0.5 in. × 0.5 in. square cross-section under a unit pure bending moment, a comparison for the axial stress along η axis at $\xi = 0$ is given in Table 5. It is clear that the present result is consistent with the analytical solution [25].

6.3. Effect of geometrical parameters of curved beam on structural behaviors

Consider a carbon/epoxy box beam with the height and width of the cross section $h = 0.05$ m and $c = 0.08$ m, respectively. The radius $a = 400$ mm. The elastic constants of ply material in computation are $E_L = 109.65$ GPa, $E_T = 7.87$ GPa, $G_{LT} = 2.92$ GPa and $\upsilon_{LT} = 0.29$.

Two lay-up configurations are considered. The first lay-up is of form of $[0_2, \pm 45°]_s$ for the vertical (web) and the horizontal (flange) panels where the 0° direction is parallel to the beam axis (referred to as the "balanced beam"). In this case, one axis of orthotropy of the laminate is along the beam axis, so no extensional–shearing coupling is present. In second lay-up formation (the "unbalanced beam"), the same laminate is applied but its axis of orthotropy is rotated 45° with respect to the beam axis, resulting in the $[45^0_2, 90^0, 0^0]_s$ lay-up. The thickness of each laminate is chosen as 0.00025 m. Using Eq. (4), the results for the stiffness coefficients of these laminates are derived as

$$A_{nn} = 122.12 \times 10^6\ \mathrm{N/m},\ A_{qq} = 31.33 \times 10^6\ \mathrm{N/m}\ \text{and}\ A_{nq} = 0.0$$

for the balanced beam, and

$$A_{nn} = 82.98 \times 10^6\ \mathrm{N/m},\ A_{qq} = 24.26 \times 10^6\ \mathrm{N/m}\ \text{and}$$
$$A^{\pm}_{nq} = 17.29 \times 10^6\ \mathrm{N/m}$$

for the unbalanced configuration. The ± sign in A_{nq} corresponds to the panels on the left-hand and right-hand sides, respectively, and also to the lower and upper skins, respectively.

For different central angles, $\beta = \frac{\pi}{6} - \pi$, two displacement components, U, V, in ξ- and η-directions at point A (see Fig. 5) at the free end of the balanced and unbalanced beams under uniformly distributed load p_η are shown in Tables 6 and 7, respectively. The magnitude of the displacements increases with an increasing central angle. Specifically, when the central angle is between $\frac{\pi}{6} - \frac{\pi}{3}$, the displacements for the balanced beam boost rapidly during this range. When the central angle is in the scope of $\frac{\pi}{2} - \frac{2\pi}{3}$, the displacements raise slowly. It is observed that in the interval for the value of the angle, i.e., $\beta = \frac{2\pi}{3} - \pi$, the displacement U will

Table 2
Bending slope of cross-ply lay-up beam under unit tip bending load ($(0°/90°)_3$, $l/h = 29$).

x (in.)	Bending slope (Rad)			
	Experiment [36,37]	Present theory	Analysis [35]	Beam FEM [38]
0.00000	0.00000000	0.00000000	0.00000000	0.00000000
5.00000	0.00045008	0.00041242	0.00037479	0.00037479
10.00000	0.00072964	0.00072964	0.00065975	0.00063286
15.00000	0.00099231	0.00099231	0.00089552	0.00084107
20.00000	0.00117972	0.00117972	0.00105067	0.00100227
25.00000	0.00127034	0.00129186	0.00115206	0.00110365

Table 3
Twist angle of cross-ply lay-up beam under unit tip torque ($(0°/90°)_3$, $l/h = 29$).

x (in.)	Twist angle (Rad)			
	Experiment [36,37]	Present Theory	Analysis [35]	Beam FEM [38]
0.00000	0.00000000	0.00000000	0.00000000	0.00000000
5.00000	0.00006050	0.00006584	0.00006940	0.00007295
10.00000	0.00012545	0.00013262	0.00014057	0.00014875
15.00000	0.00019395	0.00020430	0.00021174	0.00022420
20.00000	0.00026513	0.00027046	0.00028114	0.00030466
25.00000	0.00036477	0.00034409	0.00035231	0.00037722

Table 4
Bending slope of symmetric lay-up beam under unit tip bending load (top and bottom $(45°)_6$, sides $(45°/-45°)_3$, $l/h = 56$).

x (in.)	Bending slope (Rad)			
	Experiment [36,37]	Present theory	Analysis [35]	Beam FEM [38]
0.00000	0.00000000	0.00000000	0.00000000	0.00000000
5.00000	0.01367000	0.01426000	0.01292630	0.01497760
10.00000	0.02343000	0.02497000	0.02348000	0.02665000
15.00000	0.03094000	0.03400000	0.03168920	0.03531000
20.00000	0.03633000	0.04062000	0.03763000	0.04230000
25.00000	0.03977000	0.04536000	0.04144000	0.04629000

Table 5
A comparison for the axial stress.

η (in.)	Axial stress (psi)	
	Analytical solution [25]	Present theory
−0.2443	−50.61224	−46.98076923
−0.19494	−39.18367	−37.48846154
−0.13291	−24.89796	−25.55961538
−0.07089	−11.83673	−13.63269231
0.05443	11.83673	10.46730769
0.11646	22.85714	22.39615385
0.19367	35.10204	37.24423077
0.24177	42.44898	46.49423077

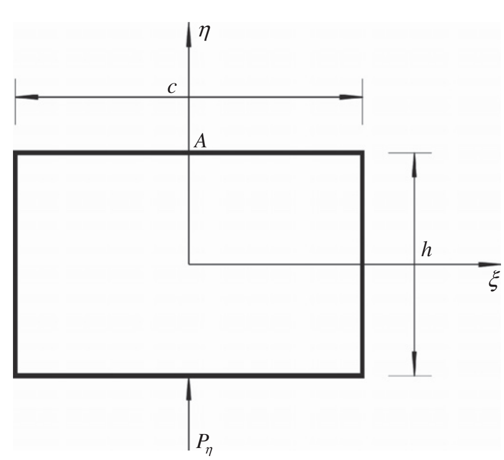

Fig. 5. Cross-section of the beam.

Table 6
Changes of displacements at point A with central angle at the free end of the balanced beam under uniformly distributed load p_η.

β (Rad)	U (m)	V (m)
$\frac{\pi}{6}$	2.45929×10^{-7}	2.34402×10^{-5}
$\frac{\pi}{3}$	1.66023×10^{-5}	2.96367×10^{-4}
$\frac{\pi}{2}$	4.0291×10^{-5}	1.44212×10^{-3}
$\frac{2\pi}{3}$	5.03119×10^{-5}	4.43411×10^{-3}
π	-1.38272×10^{-4}	1.92293×10^{-2}

Table 7
Changes of displacements at point A with central angle at the free end of the unbalanced beam under uniformly distributed load p_η.

β (Rad)	U (m)	V (m)
$\frac{\pi}{6}$	2.8056×10^{-6}	3.74493×10^{-5}
$\frac{\pi}{3}$	7.5087×10^{-6}	4.81409×10^{-4}
$\frac{\pi}{2}$	-2.937×10^{-5}	2.31487×10^{-3}
$\frac{2\pi}{3}$	-1.978×10^{-4}	6.99784×10^{-3}
π	-1.34198×10^{-3}	2.9487×10^{-2}

change to an opposite direction, which indicates that there exists a zero displacement in ξ-direction when the central angle arrives at a "critical" value between $\beta = \frac{2\pi}{3}$ and $\beta = \pi$. Obviously, the displacement V in the η-direction remains a rapid growth with a large central angle corresponding to a "flexible" beam. For the unbalanced beam, a similar trend is seen. However, for the displacement U, an increasing central angle in the scope of $\frac{\pi}{6} - \frac{\pi}{3}$ leads to a slow increase in the displacement while a relatively rapid increase of the displacements occur when central angle between $\frac{\pi}{2} - \frac{2\pi}{3}$. Moreover, it is noticed that a "critical" central angle corresponding to the zero displacement U is in the range of $\beta = \frac{\pi}{3} - \frac{\pi}{2}$, which is smaller than one for the balanced beam. In addition, the maximum values of the two displacements for the unbalanced beam are larger than the results for balanced beam, which reflects the effect of extensional–shearing coupling.

Effect of laminate thickness on the displacements is listed in Tables 8 and 9. The result indicates that the thicker the laminate is, the smaller the displacements will be. It is also seen that there is a completely opposite displacement in ξ-direction for the unbalanced beam in comparison with the case of the balanced beam. This is resulted from the different lay-up form for the beam. As shown in Tables 10 and 11, a same situation for the opposite displacement can be observed for different size of cross-section, e.g., the height. It is expected that a larger value of the height corresponds to a smaller displacement.

Table 8
Changes of displacements at point A with laminate thickness at the free end of the balanced beam under uniformly distributed load p_η.

Thickness (m)	0.00015	0.00025	0.00035	0.00045	0.00055
U ($\times 10^{-5}$) (m)	6.715	4.029	2.878	2.238	1.831
V ($\times 10^{-3}$) (m)	2.400	1.400	1.000	0.800	0.700

Table 9
Changes of displacements at point A with laminate thickness at the free end of the unbalanced beam under uniformly distributed load p_η.

Thickness (m)	0.00015	0.00025	0.00035	0.00045	0.00055
U ($\times 10^{-5}$) (m)	−4.909	−2.937	−2.094	−1.627	−1.331
V ($\times 10^{-3}$) (m)	3.900	2.300	1.700	1.300	1.100

Table 10
Changes of displacements at point A with cross-section size at the free end of the balanced beam under uniformly distributed load p_η.

Height (m)	0.03	0.05	0.07	0.09	0.11
U ($\times 10^{-5}$) (m)	8.059	4.029	2.416	1.583	1.090
V ($\times 10^{-3}$) (m)	3.700	1.400	0.800	0.500	0.300

Table 11
Changes of displacements at point A with cross-section size at the free end of the unbalanced beam under uniformly distributed load p_η.

Height (m)	0.03	0.05	0.07	0.09	0.11
U ($\times 10^{-5}$) (m)	−5.964	−2.937	−2.029	−1.629	−1.409
V ($\times 10^{-3}$) (m)	6.000	2.300	1.200	0.770	0.530

7. Conclusions

An improved model for analysis of naturally curved and twisted thin-walled beams made of anisotropic materials is proposed. The effects of initial curvature, torsion of the beams as well as torsion-related warping, transverse shear deformations and elastic coupling are included in the proposed model. The model is verified using the analytical solution and experimental data and the finite element results available. The calculation shows that the effect of extensional–shearing coupling from lay-up configuration produces large maximum values for the two displacements in the cross-section for the unbalanced beam in comparison with the results for the balanced beam without extensional–shearing coupling. Change in the central angle of the curved beam may induce a change in the direction of displacement. An increase in the laminate thickness or size of cross-section (e.g., the height, etc.) corresponds to a smaller displacement. Due to the different lay-up forms, the direction of one transverse displacement may be opposite for the balanced and unbalanced beams although the global geometry for both the beams is identical. The proposed theory can be used as an alternative model for evaluation of structural behaviors of naturally curved and twisted beams.

Acknowledgements

The authors thank the reviewers for their valuable comments and suggestions to improve the quality of the paper. The work is supported by the National Natural Science Foundation of PR China through Grant Nos. 10572105, 10972157 and Shanghai Leading Academic Discipline Project (Project No. B302).

References

[1] Schardt R. Generalized beam theory – an adequate method for coupled stability problems. Thin-Walled Struct 1994;19:161–80.
[2] Carrera E, Giunta G. Refined beam theories based on Carrera's unified formulation. Int J Appl Mech 2010;2(1):117–43.
[3] Carrera E, Giunta G, Nali P, Petrolo M. Refined beam elements with arbitrary cross-section geometries. Comput Struct 2010;88:283–93.
[4] Carrera E, Petrolo M, Nali P. Unified formulation applied to free vibrations finite element analysis of beams with arbitrary section. Shock Vib 2010;17:1–18.
[5] Carrera E, Petrolo M. On the effectiveness of higher-order terms in refined beam theories. J Appl Mech 2011;78. doi:10.1115/1.4002207.
[6] Washizu K. Some considerations on a naturally curved and twisted slender beam. J Math Phys 1964;43(2):111–6.
[7] Yu AM, Fang MX, Ma X. Theoretical research on naturally curved and twisted beams under complicated loads. Comput Struct 2002;80(32):2529–36.
[8] Yu AM, Yang XG, Nie GH. Generalized coordinate for warping of naturally curved and twisted beams with general cross-sectional shapes. Int J Solids Struct 2006;43(10):2853–67.
[9] Kolakowski Z, Krolak M. Modal coupled instabilities of thin-walled composite plate and shell structures. Comput Struct 2006;76(4):303–13.

[10] Sung-Cheon Han, Sang-Youl Lee, Guillermo Rus. Postbuckling analysis of laminated composite plates subjected to the combination of in-plane shear, compression and lateral loading. Int J Solids Struct 2006;43(18-19):5713–35.
[11] Razzaq RJ, El-Zafrany A. Non-linear stress analysis of composite layered plates and shells using a mesh reduction method. Eng Anal Bound Elem 2005;29(12):1115–23.
[12] Carrera E. On the use of the Murakami's zig-zag function in the modeling of layered plates and shells. Comput Struct 2004;82(7-8):541–54.
[13] Queiroz FD, Vellasco P, Nethercot DA. Finite element modeling of composite beams with full and partial shear connection. J Constr Steel Res 2007;63(4):505–21.
[14] Machado SP, Cortínez VH. Free vibration of thin-walled composite beams with static initial stresses and deformations. Eng Struct 2007;29(3):372–82.
[15] Liang QQ, Uy B, Richard Liew JY. Local buckling of steel plates in concrete-filled thin-walled steel tubular beam-columns. J Constr Steel Res 2007;63(3):396–405.
[16] Sapountzakis EJ, Mokos VG. 3-D beam element of composite cross section including warping and shear deformation effects. Comput Struct 2007;85(1–2):102–16.
[17] Kapania RK, Raciti S. Recent advances in analysis of laminated beams and plates, part I: shear effects and buckling, part II: vibrations and wave propagation. AIAA J 1989;27:923–46.
[18] Rehfield LW, Atilgan AR, Hodges DH. Non-classical behavior of thin-walled composite beams with closed cross-sections. J Am Helicopter Soc 1990;35:42–50.
[19] Smith EC, Chopra I. Formulation and evaluation of an analytical model for composite box beams. J Am Helicopter Soc 1991;36(3):23–35.
[20] Loughlan J, Ata M. The behavior of open and closed section carbon fiber composite beams subjected to constrained torsion. Compos Struct 1997;38(1–4):631–47.
[21] Ferrero JF, Barrau JJ, Segura JM, Castanie B, Sudre M. Torsion of thin-walled composite beams with midplane symmetry. Compos Struct 2001;54(1):111–20.
[22] Bhaskar K, Librescu L. A geometrically non-linear theory for laminated anisotropic thin-walled beams. Int J Eng Sci 1995;33(9):1331–44.
[23] Lin KC, Hsieh CM. The closed form general solutions of 2-D curved laminated beams of variable curvatures. Compos Struct 2007;79(4):606–18.
[24] Casari P, Gornet L. Characterization of residual stresses in a composite curved sandwich beam. Compos Part A: Appl Sci Manuf 2006;37(4):672–8.
[25] Yu W, Hodges DH, Volovoi V, Cesnik CES. On Timoshenko-like modeling of initially curved and twisted composite beams. Int J Solids Struct 2002;39:5101–21.
[26] Petrov E, Géradin M. Finite element theory for curved and twisted beams based on exact solutions for three-dimensional solids, part 1: beam concept and geometrically exact nonlinear formulation. Comput Methods Appl Mech Eng 1998;165(1-4):43–92.
[27] Petrov E, Géradin M. Finite element theory for curved and twisted beams based on exact solutions for three-dimensional solids, Part 2: Anisotropic and Advanced Beam Models. Comput Methods Appl Mech Eng 1998;165(1):93–127.
[28] Bauchau A, Hong CH. Large displacement analysis of naturally curved and twisted composite beams. AIAA J 1987;25(11):1469–75.
[29] Bauchau A. A beam theory for anisotropic materials. J Appl Mech 1985;107(6):416–22.
[30] El Fatmi R. On the structural behavior and the Saint Venant solution in the exact beam theory. Application to laminated composite beams. Comput Struct 2002;80(16-17):1441–56.
[31] Hyer MW. Stress analysis of fiber-reinforced composite materials. Boston: WCB/McGraw-Hill; 1998.
[32] Zhu Y, Zhang P, Yan B. Double-moment of spatial curved bars with closed thin-wall cross-section. Appl Math Mech 1999;20(12):1252–8.
[33] Bank LC, Bednarczyk PJ. A beam theory for thin-walled composite beams. Compos Sci Technol 1988;32(44):265–77.
[34] Rehfield LW, Hodges DH, Atilgan AR. Some considerations on the nonclassical behavior of thin-walled composite beams. In: Proceedings of the national technical specialists' meeting on advanced rotorcraft structures. Williamsburg (Virginia): American Helicopter Society, October 25–27, 1988.
[35] Smith EC, Chopra I. Formulation and evaluation of an analytical model for composite box beams. J Am Helicopter Soc 1991;36(3):23–35.
[36] Chandra R, Ngo H, Chopra I. Experimental study of thin-walled composite beam. In: American Helicopter Society national technical specialists' meeting on advanced rotorcraft structures. Williamsburg, Virginia, October 1988.
[37] Chandra R, Stemple AD, Chopra I. Thin-walled composite beams under bending, torsional, and extensional loads. J Aircr 1990;27(7):619–26.
[38] Kim YH, Lee SW. A solid element formulation for large deflection analysis of composite shell structures. Comput Struct 1988;30(1-2):269–74.